Mode- and bond-selective reaction of $Cl(^2P_{3/2})$ with CH_3D: C–H stretch overtone excitation near 6000 cm^{-1}

Robert J. Holiday, Chan Ho Kwon,[a] Christopher J. Annesley, and F. Fleming Crim[b]
Department of Chemistry, University of Wisconsin-Madison, Madison, Wisconsin 53706

(Received 30 May 2006; accepted 15 August 2006; published online 2 October 2006)

Experiments explore the influence of different C–H stretching eigenstates of CH_3D on the reaction of CH_3D with $Cl(^2P_{3/2})$. We prepare the $|110\rangle|0\rangle(A_1,E)$, $|200\rangle|0\rangle(E)$, and $|100\rangle|0\rangle+\nu_3+\nu_5$ eigenstates by direct midinfrared absorption near 6000 cm^{-1}. The vibrationally excited molecules react with photolytic Cl atoms, and we monitor the vibrational states of the CH_2D or CH_3 radical products by 2+1 resonance enhanced multiphoton ionization. Initial excitation of the $|200\rangle|0\rangle(E)$ state leads to a twofold increase in CH_2D products in the vibrational ground state compared to $|100\rangle|0\rangle+\nu_3+\nu_5$ excitation, indicating mode-selective chemistry in which the C–H stretch motion couples more effectively to the H-atom abstraction coordinate than bend motion. For two eigenstates that differ only in the symmetry of the vibrational wave function, $|110\rangle|0\rangle(A_1)$ and $|110\rangle|0\rangle(E)$, the ratio of reaction cross sections is 1.00 ± 0.05, showing that there is no difference in enhancement of the H-atom abstraction reaction. Molecules with excited local modes corresponding to one quantum of C–H stretch in each of two distinct oscillators react exclusively to form C–H stretch excited CH_2D products. Conversely, eigenstates containing stretch excitation in a single C–H oscillator form predominantly ground vibrational state CH_2D products. Analyzing the product state yields for reaction of the $|110\rangle|0\rangle(A_1)$ state of CH_3D yields an enhancement of 20 ± 4 over the thermal reaction. A local mode description of the vibrational motion along with a spectator model for the reactivity accounts for all of the observed dynamics. © *2006 American Institute of Physics*. [DOI: 10.1063/1.2352742]

I. INTRODUCTION

Measurements on a handful of molecules, such as water, isocyanic acid, and methane, prepared in well-characterized vibrational eigenstates have demonstrated mode- and bond-selective chemistry in H-atom abstraction reactions.[1] The key conceptual point in understanding these reactions is that eigenstates containing large components of motion along a particular reaction coordinate preferentially carry the system through the transition state along that coordinate, leading to state dependent reactivity and branching ratios. It is not always intuitively clear for polyatomic reactants which of the several vibrations should have the greatest influence on the reaction, and studies exploring the reactivity of a polyatomic molecule with different vibrations excited can reveal the details of the reaction dynamics. In favorable circumstances, understanding the subtle effects of vibrational excitation permits control over the outcome of a reactive encounter.

Theoretical[2] and experimental[3–7] studies of the reactions of Cl with CH_4 and its isotopologues have provided perhaps the most detailed view of the richness of reaction dynamics in a superficially simple system. Vibrationally driven reactions of Cl with CH_4,[8] CH_2D_2,[9] CHD_3,[10] and CD_4,[11] containing two quanta of C–H (or C–D) stretch excitation, provide clear examples of the dynamics depending on subtle details of the initial vibrational excitation. For these systems, the dynamics of the abstraction reaction are largely consistent with a spectator picture in which the bonds that do not break retain their initial vibrational excitation. For example, vibrational states that contain one quantum of stretch excitation in each of two distinct oscillators produce methyl radicals with stretch excitation, but states that have two quanta of stretch in a single oscillator react to form vibrationally unexcited methyl radicals. Such behavior, in which the surviving bonds retain their initial excitation, mimics the mode specific reactivity first observed in reactions of vibrationally excited water with H or Cl atoms.[1]

The local mode description of the initially prepared vibrational eigenstates is a useful framework for understanding the fate of the initial vibrational excitation, and it is often the case that the individual oscillators used in the local mode description remain uncoupled throughout the reaction. (The largest discrepancy between the simple local mode prediction and the experimental observation is for reaction of Cl with $CD_4(2\nu_3)$,[11] a vibration for which the local mode basis provides the poorest description of all of the methane isotopologues.[12]) Here we describe the reaction of $Cl(^2P_{3/2})$ atoms with CH_3D, a molecule that we have previously studied in the fundamental region of the C–H stretches and in the region of the first overtone of the C–D stretch.[7,13] We prepare vibrational eigenstates containing two quanta of C–H stretch excitation and observe reaction dynamics that are consistent with the spectator picture of reaction and the local mode description of the vibrational motion.

[a]Present address: Department of Chemistry, Kangwon National University, Chuncheon, Kangwon 200-701, Korea.
[b]Electronic mail: fcrim@chem.wisc.edu

TABLE I. Fundamental normal modes (fundamental frequencies taken from Ref. 20) and C–H stretch overtone and combination transitions of CH_3D. Also included are the correlations between normal modes and local modes.

Normal mode	Vibrational motion	Energy (cm^{-1})	Local mode
$\nu_1(A_1)$	Symmetric C–H stretch	2914, 2973[a]	$\|100\rangle\|0\rangle$
$\nu_2(A_1)$	C–D stretch	2200	$\|000\rangle\|1\rangle$
$\nu_3(A_1)$	CH_3 umbrella bend	1300	
$\nu_4(E)$	Antisymmetric C–H stretch	3017	$\|100\rangle\|0\rangle$
$\nu_5(E)$	CH_3 bend	1471	
$\nu_6(E)$	CH_3 rock	1155	
$2\nu_1(A_1)$	Symmetric C–H stretch overtone	5853,[b] 5834[c]	$\|200\rangle\|0\rangle$
$(\nu_1+\nu_4)(E)$	Symmetric and antisymmetric C–H stretch comb	5865,[b] 5854[c]	$\|200\rangle\|0\rangle$
$2\nu_4(A_1)$	Antisymmetric C–H stretch overtone	5980[d]	$\|110\rangle\|0\rangle$
$2\nu_4(E)$	Antisymmetric C–H stretch overtone	6022[d]	$\|110\rangle\|0\rangle$

[a]Fermi resonance interaction between ν_1 and $2\nu_5$.
[b]Reference 15.
[c]Reference 16.
[d]Reference 14.

II. BACKGROUND

A. Vibrational spectroscopy

Table I lists the fundamental and several strong C–H stretch overtone transitions of CH_3D, a prolate symmetric top molecule with C_{3v} point group symmetry. Both the A_1-and E-symmetry vibrational species are infrared active and, thus, accessible by single photon excitation. In the region of the first overtone of the C–H stretches, there are four transitions with predominantly C–H stretch character: the two symmetry components of the overtone of the antisymmetric stretch, $2\nu_4(E)$ and $2\nu_4(A_1)$, the combination of the symmetric and antisymmetric stretches, $(\nu_1+\nu_4)(E)$, and the overtone of the symmetric stretch, $2\nu_1(A_1)$. Of these four transitions, only the $2\nu_4(E)$ transition at 6022.2 cm^{-1} and the $2\nu_4(A_1)$ transition at 5980.4 cm^{-1} have assigned rotational structure.[14] In the lower energy region containing transitions to the $(\nu_1+\nu_4)(E)$ and $2\nu_1(A_1)$ states, there are several transitions with overlapping rotational structure that precludes a detailed analysis. The band origins in Table I come from experimental observation[15] or theoretical calculations.[16]

It is often useful to describe the C–H or C–D stretches as the localized motion of individual oscillators within the molecule, as Halonen and Child[17] have done using local modes for the C–H stretch overtone vibrations of CH_3D. In general, the utility of either the normal mode or the local mode descriptions depends on the size of the bond anharmonicity relative to the interbond coupling.[12,17] In local mode notation, the stretch vibrations of CH_3D are $|abc\rangle|d\rangle$, where a, b, and c are the number of quanta of stretch in each of the three equivalent C–H bonds and d is the number of quanta in the C–D stretch. Table I gives the correlation between the normal mode notation and the local mode notation for the C–H and C–D stretches, and we observe reaction of CH_3D molecules in the vibrational states that correspond to both $|110\rangle|0\rangle$ and $|200\rangle|0\rangle$ local modes. The key point in studying these vibrations is that in the local mode limit the $|110\rangle|0\rangle$ state has excitation in two C–H bonds and the $|200\rangle|0\rangle$ state has it all in one bond.

B. Reaction energetics

Figure 1 shows the energetics of the CH_3D+Cl reaction, the energies of three C–H stretching transitions in the 6000 cm^{-1} region, and the vibrational energies of the CH_2D products. Although D-atom abstraction is energetically possible even for the reaction of Cl with vibrational ground state CH_3D,[13] we omit that pathway for clarity. The only calcula-

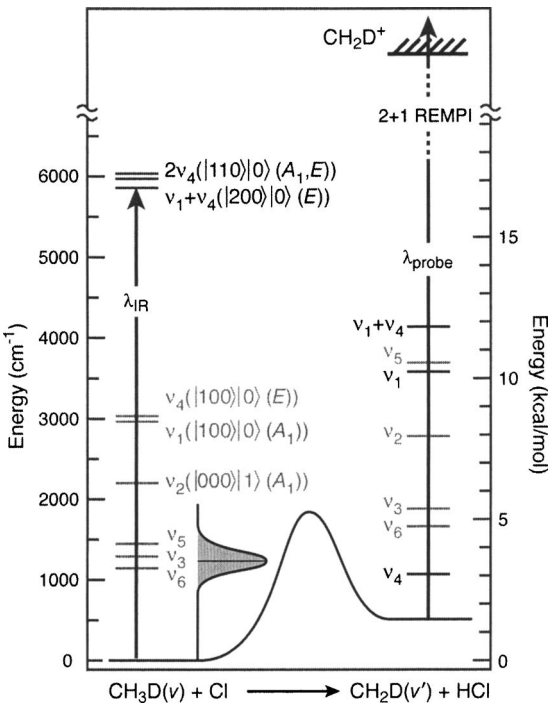

FIG. 1. Energetics of the $CH_3D+Cl \rightarrow CH_2D+HCl$ reaction. The calculated barrier height is 1809 cm^{-1} including zero-point energy corrections. The shaded curve is the collisional energy distribution of $Cl(^2P_{3/2})+CH_3D$ at a translational temperature of 10 K with its maximum at 1290 cm^{-1} and FWHM of 150 cm^{-1}. The vibrational excitation laser (λ_{IR}) excites CH_3D into one of the three vibrational eigenstates, $|110\rangle|0\rangle(A_1,E)$ and $|200\rangle|0\rangle(E)$, near 6000 cm^{-1}. Laser pulses (λ_{probe}) probe the CH_2D products by 2+1 REMPI through the 0_0^0, 1_1^1, 4_1^1, or $1_1^1 4_1^1$ resonant transitions. We also include the vibrational levels of the reactant CH_3D and the product CH_2D species, however, the shaded levels are unobserved in this work.

tion on this system, by Boone *et al.*, predicts a barrier to H-atom abstraction of 1809 cm^{-1} and an endoergicity of 514 cm^{-1} including zero-point energies.[18] The photolysis of Cl_2 generates Cl atoms with a distribution of translational energies, and the shaded curve in Fig. 1 illustrates the resulting distribution of collision energies (1290 ± 150 cm^{-1}) between $Cl(^2P_{3/2})$ and CH_3D molecules.[19] The total energy available for the products is about 6700 cm^{-1}, sufficient to populate several vibrational levels of the CH_2D and HCl ($\omega_o = 2991$ cm^{-1}) (Ref. 20) products.

We interrogate the vibrational states of the CH_2D product by 2+1 resonance enhanced multiphoton ionization (REMPI) and use the product state distributions as a window on the reactivity of $|110\rangle|0\rangle(A_1, E)$ and $|200\rangle|0\rangle(E)$ vibrational states of CH_3D. In addition, we record vibrational action spectra by monitoring one vibrational state of the CH_2D products and scanning the vibrational excitation laser wavelength. We compare the intensities of the vibrational action spectra to those of simulated absorption spectra to determine the relative reactivity of the vibrational eigenstates.

III. EXPERIMENTAL APPROACH

The experimental approach is similar to the one described previously.[13,21] We expand a 1:1:5 mixture of CH_3D (98%, Cambridge Isotope), Cl_2 (99.997%, AGA-Linde), and He (99.999%, AGA-Linde) from a glass bulb at a total pressure of 700 Torr through a pulsed solenoid valve (General Valve Series 9, 0.4 mm orifice) into a vacuum chamber and a Wiley-McLaren time-of-flight (TOF) mass spectrometer.[22] During operation the pressures are about 3×10^{-5} Torr in the vacuum chamber and 2×10^{-6} Torr in the TOF chamber. We determine a rotational temperature of 70 ± 5 K for the supersonic expansion by simulating the action spectrum of the 0_0^0 transition of CH_3 from the reaction of $CH_4(\nu_3) + Cl$ recorded under similar experimental conditions.[21]

Difference frequency generation (DFG) between the fundamental light from a Nd^{3+}:YAG (yttrium aluminum garnet) pumped dye laser and the 1064 nm Nd^{3+}:YAG fundamental in a β-barium borate (BBO) crystal provides midinfrared light near 1.7 μm (6000 cm^{-1}) for the vibrational excitation of CH_3D. We amplify the 1.7 μm light in a two-crystal, walk-off compensated[23] lithium niobate ($LiNbO_3$) optical parametric amplifier (OPA) to produce 20 mJ pulses in a bandwidth of 0.6 cm^{-1}. In addition to using the walk-off compensating configuration in our OPA, we also collinearly overlap the dye fundamental and 1064 nm laser beams through the DFG stage to prevent beam walk off when scanning the infrared wavelength. Photolysis of Cl_2 with 5 mJ of 355 nm light obtained by frequency tripling the fundamental output of another Nd^{3+}:YAG laser generates Cl atoms. Photolysis at this wavelength produces Cl atoms predominantly (>98%) in the spin-orbit ground state ($^2P_{3/2}$) with an anisotropy parameter $\beta = -1$.[24] Gently focusing the 355 nm light in the interaction region minimizes nonresonant multiphoton processes. Reactive collisions between the Cl atoms and CH_3D molecules form either CH_2D or CH_3 products. After a delay of 200 ns, we detect these products by 2+1 REMPI via the $3p^2B_1$ Rydberg state[25] for CH_2D or the $3p^2A_2''$ Rydberg state[26] for CH_3 using 2 mJ of 333 nm light generated by frequency doubling the fundamental of a Nd^{3+}:YAG pumped dye laser. We allow the CH_3^+ ($m/z = 15$) and CH_2D^+ ($m/z = 16$) ions to separate by mass in the TOF mass spectrometer and simultaneously record their yield to obtain product state distributions.

The vibrational excitation laser operates at 10 Hz and the photolysis and probe lasers at 20 Hz. Subtracting the alternating signal with only the photolysis and probe laser beams from the signal with all three laser beams present separates the reaction of the vibrational ground state CH_3D molecules (thermal reaction) from the reaction of the vibrationally excited CH_3D molecules (vibrationally enhanced reaction). When recording an action spectrum, we use a small reflection of the midinfrared light to obtain a room-temperature photoacoustic spectrum simultaneously.

IV. RESULTS AND DISCUSSION

A. Photoacoustic spectrum

Understanding the influence of vibrational excitation on the dynamics of a reactive encounter requires first identifying the vibrational transition and describing the associated nuclear motion. The photoacoustic spectrum in Fig. 2(a) is a direct measure of the absorption and illustrates the complex vibrational structure of CH_3D in the 6000 cm^{-1} region. The intensities below 5920 cm^{-1} are scaled by a factor of 2 to emphasize the rotational structure. We calibrate our experimental wave number scale by recording a photoacoustic spectrum of CH_4 and comparing it to transitions in the HITRAN database.[27] The $|110\rangle|0\rangle(A_1)$ and $|110\rangle|0\rangle(E)$ bands at 5980.4 and 6022.2 cm^{-1}, respectively, are relatively strong and isolated. The dashed vertical lines in Fig. 2(a) mark the energies for transitions that have primarily C–H stretch character calculated by Wang and Sibert using canonical Van Vleck perturbation theory (CVPT).[16]

We observe two prominent sets of transitions in the high frequency range of the spectrum and assign them to the $|110\rangle|0\rangle(A_1)$ and $|110\rangle|0\rangle(E)$ bands, in agreement with the transitions observed by Deng *et al.*[14] In the low frequency range of the spectrum, we observe at least two distinct E-symmetry transitions. The first transition at 5857 cm^{-1} is consistent with the observed band origin of the $|200\rangle|0\rangle(E)$ local mode.[15] We assign the other transition at 5766 cm^{-1} to either one or both of the symmetry components (A_1, E) of the $|100\rangle|0\rangle + \nu_3 + \nu_5$ vibration, as suggested by the CVPT calculation[16] and by the frequency measured in liquid argon (assigned to only the $|100\rangle|0\rangle(A_1) + \nu_3 + \nu_5$ transition).[15] We do not assign the remaining features in the spectrum because of limited resolution and overlapping transitions at 298 K.

B. Action spectra

The intensity observed in a photoacoustic spectrum reflects solely the infrared absorption probability, but the intensity observed in an action spectrum reflects both that infrared absorption intensity and the reaction cross section,

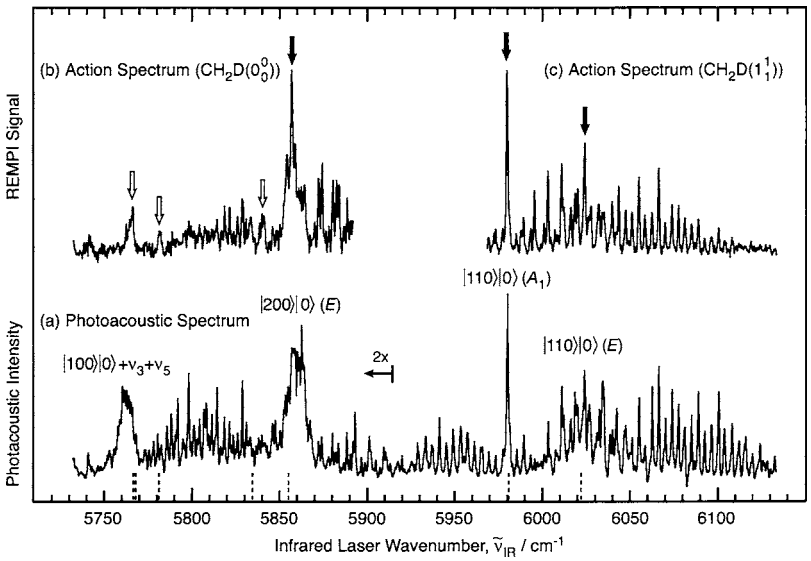

FIG. 2. (a) Photoacoustic absorption spectrum of CH_3D at 298 K. The intensity below 5920 cm^{-1} is scaled by a factor of 2 to emphasize the rotational structure. The dashed vertical lines are the transitions that have primarily C–H stretch character calculated by CVPT. (b) Action spectrum of the $CH_3D(v)+Cl$ reaction monitoring the $CH_2D(0_0^0)$ transition. The arrows show the positions of four observed transitions at 5766, 5782, 5841, and 5857 cm^{-1}. (c) Action spectrum of the $CH_3D(v)+Cl$ reaction monitoring the $CH_2D(1_1^1)$ transition. The solid arrows in (b) and (c) mark the transitions used to record the product state distributions. There is no appreciable $CH_2D(1_1^1)$ signal below 5900 cm^{-1}, nor is there $CH_2D(0_0^0)$ signal above 5950 cm^{-1}.

$$I_{\text{action}}^{\nu'} \propto I_{\text{absorption}}^{\nu'} \sigma_R^{\nu'}. \tag{1}$$

Only molecules that react to form products in the probed quantum state contribute to the action spectrum. Thus, the ratio of intensities in the action and absorption spectra at the same temperature gives the relative efficiency of a vibration in accelerating the reaction. As demonstrated below, reaction of CH_3D molecules having vibrational energy in one C–H stretch forms CH_2D radicals without any C–H stretching excitation, but reaction of CH_3D molecules with excitation in two different oscillators forms radicals with C–H stretching excitation. Consequently, action spectra taken monitoring different product states provide a view of the reactivity of different initially prepared vibrational eigenstates.

1. Ground vibrational state products

Observing *ground* vibrational state CH_2D products by monitoring the 0_0^0 transition while scanning the infrared laser wavelength gives only the transitions shown in the action spectrum in Fig. 2(b). The relatively modest cooling to about 70 K in the supersonic expansion reduces the rotational congestion compared to the room-temperature photoacoustic spectrum [Fig. 2(a)], and there are at least four distinct transitions that enhance the H-atom abstraction channel leading to ground state CH_2D products. The arrows in Fig. 2(b) mark these transitions at 5766, 5782, 5841, and 5857 cm^{-1}. Despite the simplification in the action spectrum compared to the photoacoustic spectrum, we cannot simulate the spectrum completely. The simulations of the $|200\rangle|0\rangle(E)$ band at 5857 cm^{-1} show that the experimental spectrum contains features that do not belong to the rotational structure of a single perpendicular transition of a prolate symmetric top molecule. These features may result from couplings that perturb the predicted structure or may be previously unobserved transitions that add to the spectral congestion. Nonetheless, we tentatively assign the feature at 5782 cm^{-1} to an A_1-symmetry component of the $|100\rangle|0\rangle+\nu_3+\nu_5$ vibration, in accord with the CVPT calculation.[16] The feature at 5840.9 cm^{-1} is most likely the transition to the $|200\rangle|0\rangle(A_1)$ eigenstate, in fair agreement with the predicted band origin of 5833.8 cm^{-1} (Ref. 16) and the reported frequency of 5848 cm^{-1} in liquid argon.[15] The action spectrum does not provide enough information to identify the transition at 5766.4 cm^{-1} as one symmetry component of $|100\rangle|0\rangle+\nu_3+\nu_5$ or as a mixture of both possible symmetries.

Without accurate fits to the photoacoustic spectrum, we are unable to determine the relative infrared cross sections of the various vibrational transitions needed to compare the relative reactivity of the eigenstates quantitatively. Even with the difference in temperature, it is obvious from the relative sizes of the transitions in the photoacoustic and action spectra that not all of the vibrations promote the reaction of CH_3D+Cl equally. We estimate the relative reactivity of the $|200\rangle|0\rangle(E)$ and the $|100\rangle|0\rangle+\nu_3+\nu_5$ eigenstates by comparing the maximum intensities in the two spectra to obtain

$$\frac{\sigma_R^{|200\rangle|0\rangle(E)}}{\sigma_R^{|100\rangle|0\rangle+\nu_3+\nu_5}} = \frac{I_{\text{action}}^{|200\rangle|0\rangle(E)}/I_{\text{absorption}}^{|200\rangle|0\rangle(E)}}{I_{\text{action}}^{|100\rangle|0\rangle+\nu_3+\nu_5}/I_{\text{absorption}}^{|100\rangle|0\rangle+\nu_3+\nu_5}} \approx 2.0 \pm 0.5. \tag{2}$$

This estimate rests on the intensity at 5766.4 cm^{-1} originating from only one eigenstate. The transitions to the stretching state $|200\rangle|0\rangle(E)$ and to the stretch-bend combination $|100\rangle|0\rangle+\nu_3+\nu_5$ differ by only 90 cm^{-1}, corresponding to a difference of less than 2% in the total available energy for the H-atom abstraction reaction, but the reaction probabilities of the two states differ by a factor of 2. Clearly, the state in which some of the excitation is in the bends (ν_3 and ν_5) produces less enhancement than the pure stretching state.

Determining the role of bend excitation in promoting these abstraction reactions has been difficult.[4–6,28] The most recent experiments on bend excitation in the reaction of $Cl+CH_4$ estimate a modest enhancement of 2–4 in reactivity over that of the ground vibrational state[5] in contrast to an enhancement factor of 30 for antisymmetric stretch excitation.[29] In the case of the reaction of CD_4 with Cl, Zhou *et al.* also conclude that the addition of vibrational energy to the ν_2 or ν_4 bends does not produce mode specific reactivity and is roughly equivalent to increasing the translational energy by the same amount, producing an enhancement of

about 3.[4] In the reaction of H_2O excited to either the stretching state $|03\rangle^-$ or the stretch-bend combination $|02\rangle^-|2\rangle$ at a total energy of twice the barrier, replacing one quantum of stretch with two quanta of bend decreases the reactivity by a factor of 3.[30] Here, we see similar behavior in which the combination of C–H stretch with bend excitation does not drive the hydrogen abstraction reaction as effectively as a nearly isoenergetic vibration consisting of only C–H stretch excitation, despite both having energies well above the barrier to reaction.

2. Vibrationally excited products

Observing *stretch excited* products by monitoring the $CH_2D(1_1^1)$ transition while scanning the infrared laser wavelength gives the action spectrum shown in Fig. 2(c), which contains transitions to the $|110\rangle|0\rangle(A_1)$ and $|110\rangle|0\rangle(E)$ eigenstates of CH_3D. The spectra show no clear signature of one vibration enhancing the H-atom abstraction more than the other, and a quantitative comparison of the photoacoustic spectrum and the action spectrum is possible in this case. We first simulate the spectra using the same approach as we used for the $2\nu_2$ and $\nu_3+\nu_4$ vibrations of CH_3D.[13] For the simulation of the transitions to the $|110\rangle|0\rangle(A_1)$ and $|110\rangle|0\rangle(E)$ eigenstates, we use the constants determined by Deng *et al.* for the excited states[14] along with those of Tarrago *et al.* for the vibrational ground state.[31]

Figure 3 shows the action spectrum and the photoacoustic spectrum with the corresponding simulations as well as the components from the individual transitions that go into the simulation. We normalize the experimental spectrum and the E-symmetry components to the ${}^RR_3(3)$ transition marked by the arrows in Figs. 3(a) and 3(b) and then scale the A_1-symmetry components to reproduce the complete experimental spectrum. In the simulation of the photoacoustic spectrum at 298 K, the scaling factor for the A_1-symmetry component is the ratio of the infrared cross sections for the two transitions, and in the simulation of the action spectrum at 70 K, it is the product of the relative infrared cross sections and the relative reaction cross sections. The scaling factors are the same for both the photoacoustic and action spectra, showing that the reactivity of the two symmetry components is the same. A quantitative calculation of the relative reactivity[32] gives $\sigma_R^{|110\rangle|0\rangle(A_1)}/\sigma_R^{|110\rangle|0\rangle(E)}=1.00\pm0.05$.

The identical reactivities of the A_1- and E-symmetry species of the $|110\rangle|0\rangle$ local mode starkly contrast with the behavior of CH_3D excited in the fundamental C–H stretch region.[33] In that region, only the A_1-symmetry component of the $|100\rangle|0\rangle$ local mode adiabatically correlates to a reactive mode in the reduced C_s symmetry of a collinear $Cl+CH_3D$ reactive collision. Consequently, the $|100\rangle|0\rangle(A_1)$ eigenstate is four times more reactive than the $|100\rangle|0\rangle(E)$ eigenstate. The situation is very different for the three $|110\rangle|0\rangle$ eigenstates studied here because two of the components reduce to excitation of a reactive C–H oscillator in C_s symmetry. The essential difference is that excitation of two distinct C–H oscillators that correlate to A' and A'' reactive modes makes both the A_1 and E eigenstates reactive.

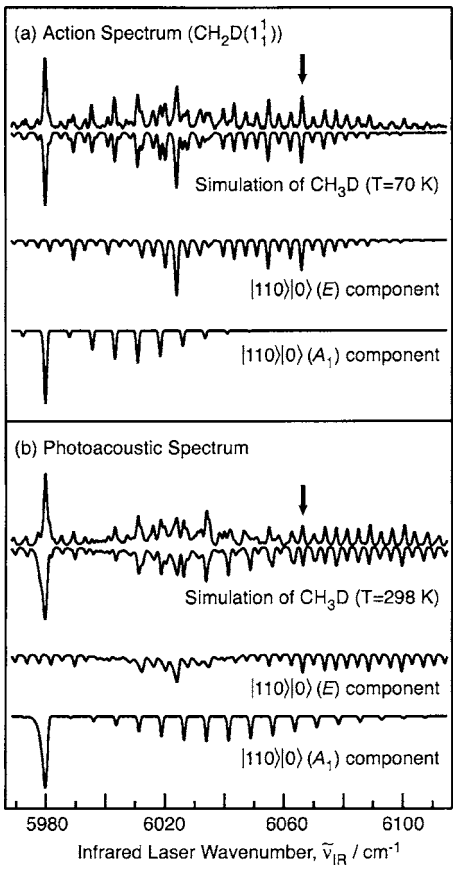

FIG. 3. (a) Experimental and simulated action spectra of $CH_3D(v)+Cl$. The simulation calculates the individual symmetry species separately and normalizes the E-symmetry component to the ${}^RR_3(3)$ transition of the action spectrum. The A_1-symmetry component is scaled and summed with the E-symmetry component to reproduce the observed action spectrum. (b) Experimental room-temperature photoacoustic and simulated absorption spectra of CH_3D. The simulation procedure is the same as for the action spectrum.

C. CH_2D product state distributions

All of the observed vibrations of CH_3D in the region of 6000 cm^{-1} involve at least one quantum of C–H stretch. Intuition suggests that C–H stretching vibration should drive the H-atom abstraction channel to yield CH_2D products. The other aspect, however, is the distribution of the available energy into the vibrational modes of the polyatomic free radical CH_2D. The spectra in Fig. 4 show the partitioning of the methyl radical products between two vibrational states for the reaction of $CH_3D(v)$ with Cl. We record these spectra by fixing the infrared laser at the most intense features of the transitions to the $|110\rangle|0\rangle(E)$, $|110\rangle|0\rangle(A_1)$, and $|200\rangle|0\rangle(E)$ eigenstates in the action spectra [marked by solid arrows in Figs. 2(b) and 2(c)].

Figure 4(d) shows the mass-resolved (2+1) REMPI spectra of the products of the thermal reaction, $CH_3D(v=0)+Cl$, obtained by simultaneously monitoring CH_2D (upper trace) and CH_3 (lower trace) products. The maximum in the upper trace at a two-photon energy of 59 929 cm^{-1} comes from ionizing the vibrational ground state of CH_2D through the 0_0^0 transition of the $3p^2B_1$ Rydberg state.[25] In the lower trace, we identify the feature at 59 944 cm^{-1} as the 0_0^0 band of the $3p^2A_2''$ Rydberg state of CH_3.[26] The observation of both

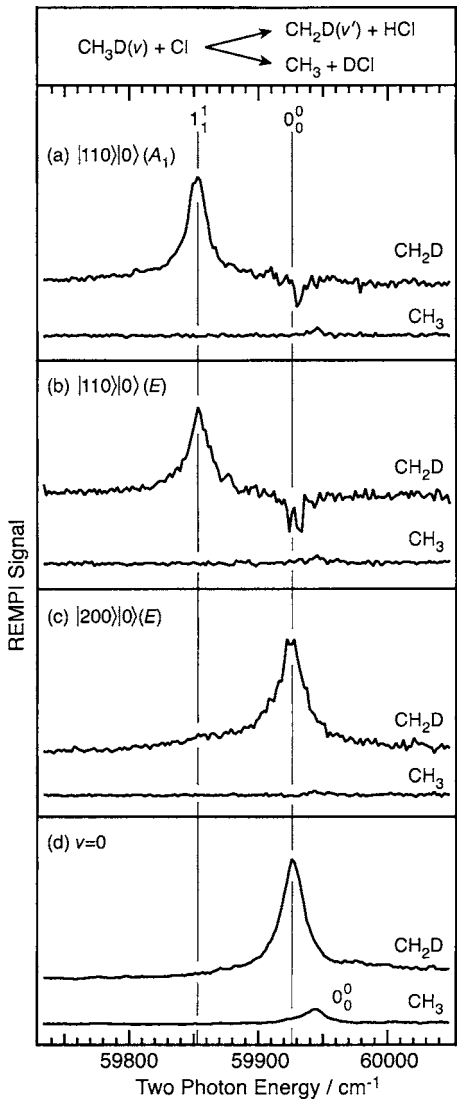

FIG. 4. Mass-resolved 2+1 REMPI product state distributions for initial excitation of (a) the $|110\rangle|0\rangle(A_1)$, (b) the $|110\rangle|0\rangle(E)$, and (c) the $|200\rangle|0\rangle(E)$ states. (d) Mass-resolved 2+1 REMPI product state distribution of the thermal reaction, $CH_3D(v=0)+Cl$. The light vertical lines mark the 0_0^0 and 1_1^1 transitions in the 2+1 REMPI of CH_2D. We simultaneously record the CH_2D^+ and CH_3^+ signals for each reaction.

$CH_2D(0_0^0)$ and $CH_3(0_0^0)$ transitions indicates that there is sufficient energy in the collisions between Cl and vibrational ground state CH_3D to surmount the reaction barriers for the H- and D-atom abstraction. As discussed previously,[13] the calculation reported in Fig. 1 significantly overestimates the actual barrier. Unknown Franck-Condon factors prevent a quantitative determination of the branching ratio between the two pathways, but the sixfold smaller $CH_3(0_0^0)$ intensity is consistent with the primary kinetic isotope effect and the larger number of hydrogen atoms compared to deuterium atoms.

We observe only enhanced H-atom abstraction for all of the eigenstates containing C–H stretching excitation, but the vibrational energy content of the CH_2D product depends strongly on the details of the initially excited eigenstate. Figure 4(c) shows that initial excitation of the $|200\rangle|0\rangle(E)$ eigenstate leads to formation of CH_2D products in their ground vibrational states. By contrast, reaction of Cl atoms with CH_3D molecules in the $|110\rangle|0\rangle(E)$ and $|110\rangle|0\rangle(A_1)$ eigenstates yields vibrationally excited CH_2D fragments, as shown by the presence of the 1_1^1 transition in Figs. 4(a) and 4(b). [We have previously assigned the feature at 59 852 cm^{-1} to this transition for CH_2D products with C–H stretch excitation[13] and have confirmed this assignment by *ab initio* calculations (Table II) on ground and the intermediate Rydberg state (which we approximate as the corresponding ion).[32]]

We also observe some of the products in an excited bending state (ν_4), consistent with the change of the initially tetrahedral CH_3D molecule into the planar CH_2D fragment. Figure 5 shows the REMPI spectrum of the products including the 1_1^1 transition at a two-photon wave number of 59 852 cm^{-1} and a new transition, $1_1^1 4_1^1$, for the bend excited fragment at 60 560 cm^{-1}.[32] For comparison, we also show the analogous pair of transitions for the products from the reaction of $CH_3D(|100\rangle|0\rangle(E))$,[34] which has only a single C–H stretch excited. Consistent with the spectator model of the reaction, both initial states produce roughly comparable fractions (30%–40%) of bend excited fragments, with or without an extra quantum of C–H stretching excitation depending on the initial excitation in the spectator bond.

The spectator picture of reaction dynamics rests on the assumption that each bond of the reactant behaves as an isolated oscillator, allowing the surviving bond to retain its initial vibrational motion. The $|200\rangle|0\rangle(E)$ vibration has only a single C–H oscillator excited, and coupling this motion to the reaction coordinate leads to CH_2D products without C–H stretch excitation. The $|110\rangle|0\rangle(A_1,E)$ eigenstates, on the other hand, have two excited C–H bonds, only one of which breaks during the abstraction reaction and leaves stretch excited CH_2D products behind. The product state yields in Fig. 4 support the spectator picture of reaction of vibrationally excited CH_3D molecules with Cl atoms.

D. Reaction enhancement for C–H stretch excitation

The spectra in Figs. 4(a) and 4(b) show that the $CH_2D(0_0^0)$ product signal decreases upon excitation of the $|110\rangle|0\rangle(A_1,E)$ eigenstates. Reactions of $CHD_3(\upsilon_1=1,2)$ with Cl show this same behavior.[10] The reduction in the amount of the thermal reaction product is consistent with pure spectator behavior in which the vibrational excitation of the reactant reduces the number of ground vibrational state molecules available to react. To estimate the enhancement factor for reaction of molecules in the $|110\rangle|0\rangle(A_1)$ state compared to the vibrational ground state of CH_3D, we fit the spectra in Figs. 4(a) and 4(d) using Lorentzian line shapes and determine the area of each band. We assume that the depletion of the $CH_2D(0_0^0)$ feature directly reflects the fraction of molecules excited to the $|110\rangle|0\rangle(A_1)$ eigenstate and that the Franck-Condon factors are the same for the 1_1^1 and 0_0^0 transitions. The ratio of the area of the 1_1^1 transition to that of the negative going 0_0^0 transition in Fig. 4(d) is 13±3. This value, however, does not account for the differences in product state distributions where reaction of ground state CH_3D forms exclusively CH_2D products in their ground vibrational state.[13] If we use the relative amounts of ground state and

TABLE II. The calculated normal mode frequencies for CH_2D (C_{2v}) and CH_2D^+ (C_{2v}). Calculations are at the MP2 level of theory with a 6-311++G(2*d*,2*p*) basis set and the results are scaled by the recommended factor of 0.9434. All frequencies are in units of cm^{-1}.

		CH_2D (C_{2v})		CH_2D^+ (C_{2v})	
Normal mode	Vibrational motion	Expt.	Calc.	Expt.[a]	Calc.
$\nu_1(A_1)$	Symmetric C–H stretch	3069[b]	3069	2995, 3005	2995
$\nu_2(A_1)$	C–D stretch		2269	2220	2224
$\nu_3(A_1)$	Scissors		1367		1369
$\nu_4(B_1)$	OPLA	555[a]	415	1260	1274
$\nu_5(B_2)$	Antisymmetric C–H stretch		3176	3106	3110
$\nu_6(B_2)$	C–D bend		1161		1221

[a]Reference 25.
[b]Reference 13.

bend excited products calculated above for the reaction of $CH_3D(|110\rangle|0\rangle(A_1))$, we obtain an enhancement of

$$\frac{\sigma_R^{|110\rangle|0\rangle(A_1)}}{\sigma_R^{v=0}} = 20 \pm 4, \tag{3}$$

for reaction of the $|110\rangle|0\rangle(A_1)$ state compared to the thermal reaction.

For the reaction of $Cl+CH_4$, initial excitation of the antisymmetric C–H stretch (ν_3) (Ref. 29) and the symmetric C–H stretch-bend combination $(\nu_1+\nu_4)$ (Ref. 21) enhance the hydrogen abstraction reaction by factors of 30 and 19, respectively. In a local mode picture, each of these states corresponds to excitation of a single C–H oscillator,[12] but the $|110\rangle|0\rangle(A_1)$ state of CH_3D corresponds to excitation of two distinct oscillators. These three cases show that excitation of a single C–H oscillator gives roughly the same enhancement compared to the inefficient thermal reaction regardless of excitation in the spectator bonds.

V. SUMMARY

Our experimental studies of the dynamics of the reaction of CH_3D molecules in vibrational eigenstates near 6000 cm^{-1} with Cl clearly show the effect of different initial nuclear motion on the H-atom abstraction reactions. Excitation of two of the states, corresponding to the A_1- and *E*-symmetry components of the $|110\rangle|0\rangle$ local mode, leads to C–H *stretch excited* CH_2D fragments, and excitation of four other states, which we assign as the two symmetry species of the $|200\rangle|0\rangle$ and $|100\rangle|0\rangle+\nu_3+\nu_5$ eigenstates, leads to CH_2D *without* C–H stretch excitation. All of these vibrations contain C–H motion and produce bond-selective reaction by enhancing the hydrogen abstraction channel.

The vibrational action spectra show that the $|200\rangle|0\rangle(E)$ eigenstate is twice as reactive as the $|100\rangle|0\rangle+\nu_3+\nu_5$ state. The observed mode selectivity supports the intuitive idea that C–H stretching motion enhances the abstraction reaction more effectively than bending motion. For the A_1- and *E*-symmetry species of the $|110\rangle|0\rangle$ vibration, we quantitatively compare the relative reaction cross sections by fitting the observed photoacoustic and action spectra to obtain identical reaction cross sections. The local mode behavior of two distinct C–H oscillators determines the reactivity, which is independent of the symmetry of the vibrational wave function.

We observe product state populations that indicate that local modes containing C–H excitation in two oscillators lead exclusively to CH_2D products with C–H stretch excitation. Conversely, local modes with only one C–H bond excited drive the abstraction channel leading to $CH_2D(v=0)$ radicals. For initial excitation of the $|110\rangle|0\rangle(A_1)$ state, we also observe a new transition in the 2+1 REMPI spectrum of CH_2D that we assign to the $1_1^1 4_1^1$ band. In addition, we obtain an enhancement factor of 20±4 for reaction of the $|110\rangle|0\rangle(A_1)$ state relative to the thermal reaction, consistent with the observed enhancement for eigenstates with one quantum of C–H excitation in the reaction of CH_4+Cl. The similarity in the branching ratios and enhancement factors illustrates that a single excited oscillator determines the reactivity and that additional excitation of an uncoupled oscillator remains in the surviving bond.

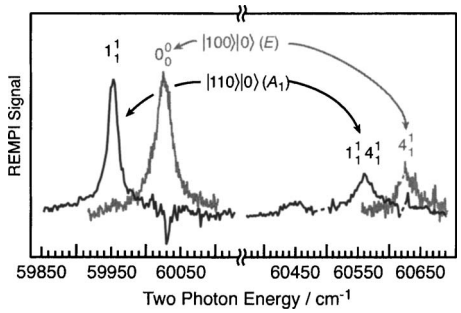

FIG. 5. Mass-resolved 2+1 REMPI spectra of the $CH_2D(v)$ products for the reactions of $CH_3D(|110\rangle|0\rangle(A_1))+Cl$ (this work) and $CH_3D(|100\rangle|0\rangle(E))+Cl$ (Ref. 34).

ACKNOWLEDGMENTS

We gratefully acknowledge the support of this work provided by the National Science Foundation. We thank Professor E. L. Sibert for very helpful discussions, and we thank both Professor Sibert and Professor Wang for use of their unpublished calculations.

[1] F. F. Crim, Acc. Chem. Res. **32**, 877 (1999).
[2] W. T. Duncan and T. N. Truong, J. Chem. Phys. **103**, 9642 (1995); J. Espinosa-Garcia and J. C. Corchado, *ibid.* **105**, 3517 (1996); H.-G. Yu

and G. Nyman, Phys. Chem. Chem. Phys. **1**, 1181 (1999); J. Chem. Phys. **110**, 7233 (1999); J. C. Corchado, D. G. Truhlar, and J. Espinosa-Garcia, *ibid.* **112**, 9375 (2000).
[3] C. Murray and A. J. Orr-Ewing, Int. Rev. Phys. Chem. **23**, 435 (2004); B. Zhang and K. Liu, J. Chem. Phys. **122**, 101102 (2005).
[4] J. Zhou, J. J. Lin, B. Zhang, and K. Liu, J. Phys. Chem. A **108**, 7832 (2004).
[5] H. A. Bechtel, J. P. Camden, D. J. A. Brown, M. R. Martin, R. N. Zare, and K. Vodopyanov, Angew. Chem., Int. Ed. **44**, 2382 (2005).
[6] Z. H. Kim, H. A. Bechtel, J. P. Camden, and R. N. Zare, J. Chem. Phys. **122**, 084303 (2005).
[7] S. Yoon, R. J. Holiday, and F. F. Crim, J. Phys. Chem. B **109**, 8388 (2005).
[8] Z. H. Kim, H. A. Bechtel, and R. N. Zare, J. Chem. Phys. **117**, 3232 (2002).
[9] H. A. Bechtel, Z. H. Kim, J. P. Camden, and R. N. Zare, J. Chem. Phys. **120**, 791 (2004).
[10] J. P. Camden, H. A. Bechtel, D. J. Ankeny Brown, and R. N. Zare, J. Chem. Phys. **124**, 034311 (2006).
[11] H. A. Bechtel, Z. H. Kim, J. P. Camden, and R. N. Zare, Mol. Phys. **103**, 1837 (2005).
[12] L. Halonen and M. S. Child, Mol. Phys. **46**, 239 (1982).
[13] S. Yoon, R. J. Holiday, and F. F. Crim, J. Chem. Phys. **119**, 4755 (2003).
[14] K. Deng, X. Wang, H. Lin, D. Wang, and Q. Zhu, Mol. Phys. **97**, 787 (1999).
[15] V. M. Blunt, A. Brock, and C. ManzanaresI, J. Phys. Chem. **100**, 4413 (1996).
[16] X.-G. Wang and E. L. Sibert III (private communication).
[17] L. Halonen and M. S. Child, J. Chem. Phys. **79**, 4355 (1983).
[18] G. D. Boone, F. Agyin, D. J. Robichaud,F.-M. Tao, and S. A. Hewitt, J. Phys. Chem. A **105**, 1456 (2001).
[19] W. J. van der Zande, R. Zhang, R. N. Zare, K. G. McKendrick, and J. J. Valentini, J. Phys. Chem. **95**, 8205 (1991).
[20] NIST Chemistry WebBook, http://webbook.nist.gov/chemistry
[21] S. Yoon, S. Henton, A. N. Zivkovic, and F. F. Crim, J. Chem. Phys. **116**, 10744 (2002).
[22] W. W. Wiley and I. H. McLaren, Rev. Sci. Instrum. **26**, 1150 (1955).
[23] D. J. Armstrong, W. J. Alford, T. D. Raymond, A. V. Smith, and M. S. Bowers, J. Opt. Soc. Am. B **14**, 460 (1997).
[24] Y. Matsumi, K. Tonokura, and M. Kawasaki, J. Chem. Phys. **97**, 1065 (1992).
[25] J. L. Brum, R. D. Johnson III, and J. W. Hudgens, J. Chem. Phys. **98**, 3732 (1993).
[26] J. W. Hudgens, T. G. DiGiuseppe, and M. C. Lin, J. Chem. Phys. **79**, 571 (1983).
[27] L. S. Rothman, D. Jacquemart, A. Barbe *et al.*, J. Quant. Spectrosc. Radiat. Transf. **96**, 139 (2005).
[28] S. A. Kandel and R. N. Zare, J. Chem. Phys. **109**, 9719 (1998).
[29] W. R. Simpson, T. P. Rakitizis, S. A. Kandel, A. J. Orr-Ewing, and R. N. Zare, J. Chem. Phys. **103**, 7313 (1995).
[30] A. Sinha, J. D. Thoemke, and F. F. Crim, J. Chem. Phys. **96**, 372 (1992).
[31] G. Tarrago, M. Delaveau, L. Fusina, and G. Guelachvili, J. Mol. Spectrosc. **126**, 149 (1987).
[32] R. J. Holiday, Ph.D. thesis, University of Wisconsin-Madison, 2006.
[33] S. Yoon, R. J. Holiday, E. L. Sibert, and F. F. Crim, J. Chem. Phys. **119**, 9568 (2003).
[34] S. Yoon, Ph.D. thesis, University of Wisconsin-Madison, 2003.